University of Groningen

The lncRNA KTN1-AS1 co-regulates a variety of Myc-target genes and enhances proliferation of Burkitt lymphoma cells

Winkle, Melanie; Tayari, Mina M; Kok, Klaas; Duns, Gerben; Grot, Natalia; Kazimierska, Marta; Seitz, Annika; Jong, Debora; Koerts, Jasper; Diepstra, Arjan

IMPORTANT NOTE: You are advised to consult the publisher's version (publisher's PDF) if you wish to cite from it. Please check the document version below.

Document Version
Publisher's PDF, also known as Version of record

Link to publication in University of Groningen/UMCG research database

The lncRNA KTN1-AS1 co-regulates a variety of Myc-target genes and enhances proliferation of Burkitt lymphoma cells

Melanie Winkle[1,2,*], Mina M Tayari[1,3], Klaas Kok[4], Gerben Duns[5], Natalia Grot[6], Marta Kazimierska[6], Annika Seitz[1], Debora de Jong[1],

Jasper Koerts[1], Arjan Diepstra[1], Agnieszka Dzikiewicz-Krawczyk[6], Christian Steidl[5], Joost Kluiver[1] and Anke van den Berg[1]

[1]Department of Pathology and Medical Biology, University of Groningen, University Medical Center Groningen (UMCG), Groningen, the Netherlands
[2]Department of Translational Molecular Biology, University of Texas MD Anderson Cancer Center, Houston, TX, USA
[3]Department of Human Genetics, University of Miami, Sylvester Comprehensive Cancer Center, Miami, FL, USA
[4]Department of Genetics, University of Groningen, University Medical Center Groningen (UMCG), Groningen, the Netherlands
[5]Department of Lymphoid Cancer Research, BC Cancer Center, Vancouver, BC, Canada
[6]Institute of Human Genetics, Polish Academy of Sciences, Poznan, Poland
*To whom correspondence should be addressed at: Department of Translational Molecular Pathology, The University of Texas MD Anderson Cancer Center, 2130 W Holcombe Blvd, LSP9.3019, Houston, TX 77030, USA. Tel: +1 (713) 792 0899; Email: mwinkle@mdanderson.org

Abstract

Long non-coding RNAs (lncRNAs) are involved in many normal and oncogenic pathways through a diverse repertoire of transcriptional and posttranscriptional regulatory mechanisms. LncRNAs that are under tight regulation of well-known oncogenic transcription factors such as c-Myc (Myc) are likely to be functionally involved in their disease-promoting mechanisms. Myc is a major driver of many subsets of B cell lymphoma and to date remains an undruggable target. We identified three Myc-induced and four Myc-repressed lncRNAs by use of multiple *in vitro* models of Myc-driven Burkitt lymphoma and detailed analysis of Myc binding profiles. We show that the top Myc-induced lncRNA KTN1-AS1 is strongly upregulated in different types of B cell lymphoma compared with their normal counterparts. We used CRISPR-mediated genome editing to confirm that the direct induction of KTN1-AS1 by Myc is dependent on the presence of a Myc E-box-binding motif. Knockdown of KTN1-AS1 revealed a strong negative effect on the growth of three BL cell lines. Global gene expression analysis upon KTN1-AS1 depletion shows a strong enrichment of key genes in the cholesterol biosynthesis pathway as well as co-regulation of many Myc-target genes, including a moderate negative effect on the levels of Myc itself. Our study suggests a critical role for KTN1-AS1 in supporting BL cell growth by mediating co-regulation of a variety of Myc-target genes and co-activating key genes involved in cholesterol biosynthesis. Therefore, KTN1-AS1 may represent a putative novel therapeutic target in lymphoma.

Introduction

Long non-coding (lnc)RNAs have gained much attention as novel modulators of normal and cancer cell physiology. Through diverse transcriptional and post-transcriptional regulatory roles, lncRNAs partake in many known (oncogenic) pathways. LncRNAs are often expressed in a cell-type specific manner (1,2) and cancer cell-specific expression patterns have been reported (3). Therefore, studying lncRNA function can potentially lead to an expansion of druggable targets for cancer treatment.

The oncogenic transcription factor Myc plays important roles in several subtypes of B-cell lymphoma. Burkitt lymphoma (BL) is characterized by a translocation involving the *MYC* gene locus and the immunoglobulin heavy or light chain gene loci, resulting in high levels of Myc protein. *MYC* rearrangements occur in ~10% of the diffuse large B-cell lymphoma (DLBCL) cases, while these rearrangements are less common in mantle cell, plasmablastic lymphoma and some low-grade lymphomas (4,5). Importantly, overexpression of Myc confers additional aggressiveness to these malignancies and is associated with poor prognosis (6,7).

Myc overexpression affects a large number of genes that are amongst others involved in metabolism, biosynthesis, growth, cell cycle or survival (8,9). A substantial number of the affected genes are lncRNA transcripts that are either induced (10,11) or repressed (12) by Myc (for global analyses of Myc-regulated lncRNAs see (13–15)). Furthermore, lncRNAs can regulate Myc expression or activity at the transcriptional (16–19) and post-transcriptional level (20,21) (reviewed in 22,23).

In this study, we used multiple *in vitro* models and Myc binding profile analysis to identify lncRNAs that are directly regulated by Myc. This resulted in the discovery of the Myc-induced lncRNA KTN1-AS1 in BL. KTN1-AS1 knockdown had a strong negative effect on cell growth and co-regulated many genes that were also affected

by knockdown of Myc itself. Our data suggest a significant co-regulation of Myc-target genes by KTN1-AS1 and showed a critical role of KTN1-AS1 in supporting BL cell growth.

Results
BL cell lines are addicted to MYC expression

Myc was expressed in all three BL cell lines tested (ST486, CA46 and DG75) at the mRNA and protein level (Supplementary Material, Fig. S1A). To confirm the dependency of these cell lines on Myc, we determined the effect of shRNA-mediated MYC inhibition on cell growth. The efficacy of two shRNAs against MYC was demonstrated by a 60–80% decrease at the protein level compared with a non-targeting control (Supplementary Material, Fig. S1B). Moreover, three known Myc-induced genes (CAD, TFAM and PGK1) (24) showed a consistent decrease in expression upon shRNA treatment (Supplementary Material, Fig. S1C). The growth of all three cell lines strongly decreased upon Myc depletion, as shown by the highly significant decreases in GFP+ cells in GFP competition assays ($P < 0.0001$) with the strongest growth inhibition in ST486 cells (Supplementary Material, Fig. S1D). These data confirm the addiction of all three BL cell lines to the Myc protein.

Identification of Myc-regulated lncRNA loci in ST486 cells

To reliably identify Myc-regulated lncRNA transcripts, we focused on gene loci consistently identified as being Myc-responsive as well as bound by Myc near their promoter. To this end, we selected transcripts that (i) showed altered expression levels in response to Myc knockdown in ST486 BL cells, (ii) showed an early (4 h), and thus likely direct response to Myc induction in P493–6 B cells (i.e. lymphoblastoid cells with a Myc-Tet-off system) (15), (iii) were directly bound by Myc across five BL cell lines (ChIP-seq) (25) and (iv) possess a Myc binding motif (i.e. 'Myc E-Box'; see Materials and Methods).

To validate the feasibility of our approach, we first assessed the selection procedure on protein coding genes (Supplementary Material, Fig. S2). Overall expression changes observed in ST486 cells upon Myc knockdown showed a highly significant overlap with a previously identified set of core target genes of Myc (gene set enrichment analysis, GSEA; FDR q value < 0.0001; Supplementary Material, Fig. S2A). A total of 1073 protein coding genes responded to Myc-knockdown in ST486 cells (Supplementary Material, Fig. S2B), with 503 (47%) Myc-induced and 570 (53%) Myc-repressed genes. Of the Myc-induced genes, 208 (41%) showed an early response to Myc induction in P493–6 cells, representing putative direct target genes. Indeed, 79% of these early-induced genes were also bound by Myc across 5 different BL cell lines. Myc binding near early-induced genes occurred significantly more often compared to late ($P = 0.0013$) and non-responsive genes ($P = 3 \times 10^{-17}$). Moreover, early

but not late, Myc-induced genes showed significant enrichment for the presence of the canonical Myc E-box motif 'CACGTG' (47 of 165 genes; $P = 0.044$). By applying the exact same analysis pipeline to Myc-repressed genes (Supplementary Material, Fig. S2B), we observed that only 19% of the ST486 Myc-repressed genes were also early-repressed in P493–6 cells. The majority of the ST486 Myc-repressed genes were late-repressed (41%) or non-responsive (38%) in P493–6 cells. We did not observe a significant enrichment of Myc-binding or binding motifs in early compared with late or non-responding Myc-repressed genes. Heatmaps of the coding genes fulfilling all four criteria (47 Myc-induced, 2 Myc-repressed) are shown in Supplementary Material, Fig. S2C. Of the Myc-induced coding genes, 57% (27 of 47) were previously defined as core target genes of Myc (MYC hallmarks) or Myc-targets in B cells (Daudi and P493–6) (26,27)) (Supplementary Material, Fig. S2C). Altogether, these data show that our approach reliably identifies genes directly induced by Myc.

The same selection strategy was applied to lncRNA genes (Fig. 1A) and resulted in the identification of 313 Myc-regulated probes in ST486 BL cells, of which 111 (35%) were Myc-induced and 202 (65%) were Myc-repressed. Overlap of these genes with early-response genes in P493–6 revealed 24 Myc-induced and 11 Myc-repressed probes. Heatmaps of genes are shown in Figure 1B. Seven of these lncRNA loci (detected by 9 probes) showed evidence of Myc-binding within 5 kb of their transcription start site (TSS) and had one or multiple canonical or non-canonical E-box motifs (Table 1). Among the 7 lncRNA loci, KTN1-AS1, a multi-exonic lncRNA transcript located in bidirectional orientation with the coding gene *kinectin 1* (*KTN1*), had a non-canonical E-box motif located directly at its TSS (Fig. 1C).

KTN1-AS1 is a direct transcriptional target of Myc in BL

To further support a direct regulation of KTN1-AS1 by Myc, we assessed its expression changes in P493–6 B cells at varying levels of Myc expression. To this end, we treated the cells with different concentrations of tetracycline (Tet) to achieve either full (i.e. at 0.1 μg/μl tet) or partial inhibition (i.e. at 0.1 ng/μl and 0.05 ng/μl tet) of Myc expression (Fig. 2A). KTN1-AS1 as well as the known Myc-induced genes CAD, TFAM and PGK1 showed decreased levels following the same pattern as Myc. Conversely, KTN1 did not respond to MYC inhibition (Fig. 2A). These data indicate that KTN1-AS1, but not its downstream neighbor KTN1, is a direct transcriptional target of Myc.

Next, we employed the CRISPR/Cas9 system to disrupt the integrity of the E-box sequence (28) located at the start of KTN1-AS1 exon 1. Two single guide (sg)RNAs were designed to introduce a cut within the 6-nucleotide E-box sequence (sg-MYC-E1 and sg-MYC-E2; Fig. 1C). The sgRNAs caused indels of 1–2 basepairs (bp) around the cutting site in the vast majority of ST486, CA46 and
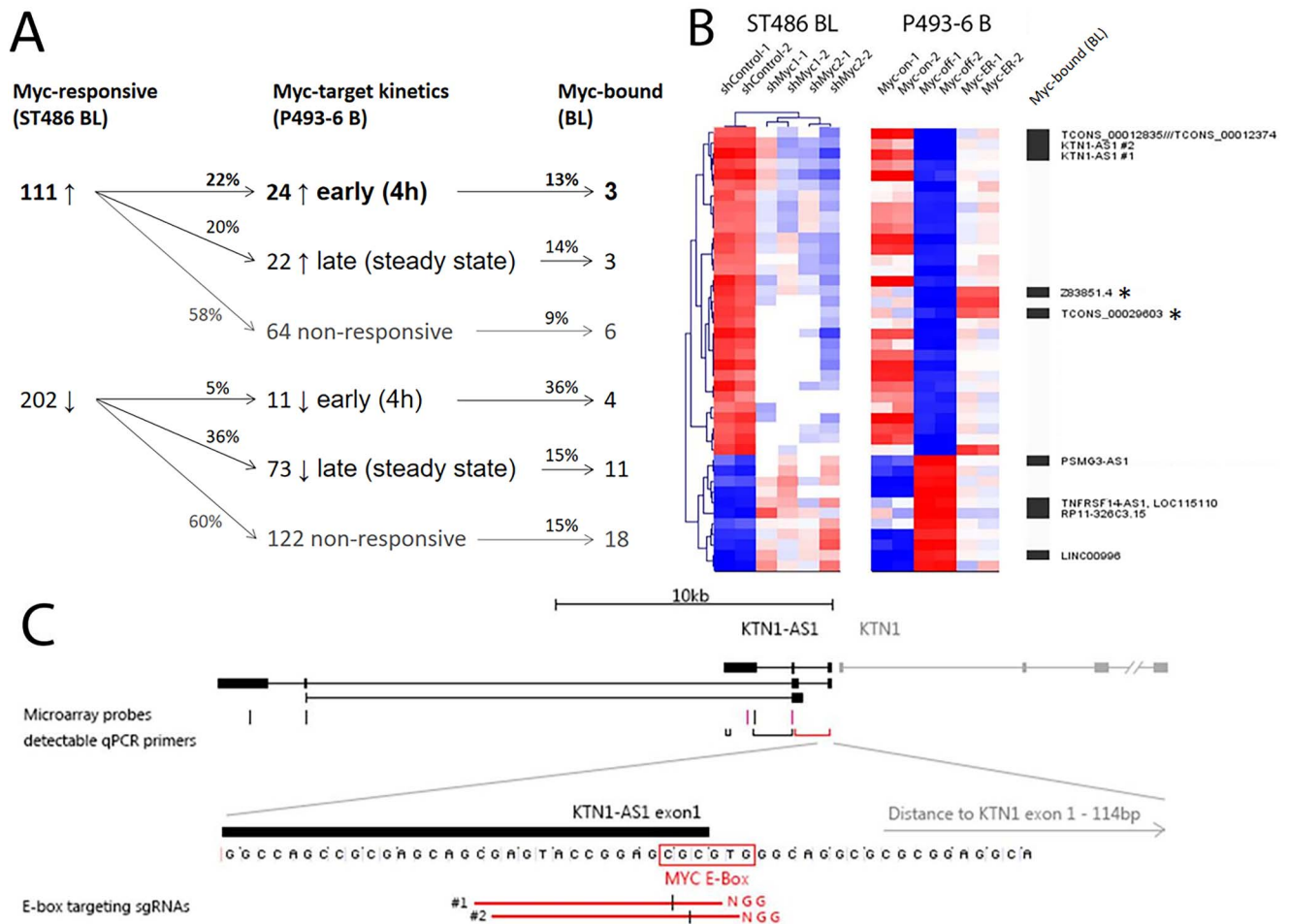
Figure 1. KTN1-AS1 is a lncRNA directly induced by Myc. (**A**) Flowchart of Myc-regulated lncRNA candidate selection based on Myc knockdown in ST486 BL cells, Myc-target kinetics in P493–6 B cells and Myc binding in BL cell lines. (**B**) Heatmap of the Myc-induced ($n = 24$) and Myc-repressed ($n = 11$) lncRNAs that are also defined as early responders in P493–6 B cells. Black bars indicate lncRNA transcripts that are also directly bound my Myc in BL cell lines. *Z83851.4 and TCONS_00029603 originate from the same locus. Red indicates high expression; blue indicates low expression. Two biological replicates are shown per infected construct. (**C**) Schematic of the KTN1-AS1 locus, the lncRNA that shows the closest association with Myc binding, possessing a Myc-binding motif (i.e. E-box) at the start of the transcribed sequence. Microarray probes (red = Myc-responsive), qPCR primers (red = standard primers used throughout this manuscript) and E-box targeting sgRNAs with PAM sequence (NGG) and cutting site are indicated. Myc-ER = Myc-early responders (P493–6).

**Table 1.** LncRNAs identified as putative direct targets of Myc

LncRNA	ST498 (fold change)	P493–6 early (fold change)	P493–6 late (fold change)	Distance TSS—Myc BS (bp)$	Distance TSS—E-box (bp)
KTN1-AS1*	2.8	9.8	15.9	(+) 82	(+) 0 [CACGCG]
Z83851.4; TCONS_00029603*	1.9	5.4	3.4	(+) 4841	(+) 3507 [CATGTG]
TCONS_00012835; TCONS_00012374	1.8	15.3	50.7	(+) 1094	(+) 557 [**CACGTG**]; (+) 1011 [CACGTT]; (+) 1097 [CACGCG]; (+) 1115 [CACGAG]
LINC00996	−4.1	−2.3	−13.2	(−) 1957	(−) 1021 [**CACGTG**]; (+) 557 [**CACGTG**]
RP11-326C3.15	−3.6	−5.5	−5.1	(+) 1123	(−) 280 [CACGTT]; (+) 553 [CACGAG]
TNFRSF14-AS1; LOC115110	−3.1	−3.5	−3.9	(−) 2939	(−) 2902 [**CACGTG**]; (+) 319 [**CACGTG**]
PSMG3-AS1	−1.8	−5.5	−9.0	(−) 37	(−) 23 [CACGCG]; (−) 134 [CACGCG]; (−) 225 [CACGTT]

$indicates distance TSS to the center of a (broader) ChIP signal peak. *mean fold change of two probes is shown. Canonical E-box motif indicated in **bold**, for non-canonical motifs the nucleotides differing from canonical sequence are indicated in red.

P493–6 cells. A minority of the cells carried larger deletions (~7–14 bp; TIDE analysis (29), data not shown). The overall efficiency of the sgRNAs was >95% in ST486 and ~80% in CA46 and P493–6 cells. We observed a consistent decrease in KTN1-AS1 of 56 and 72% in Myc-on P493–6 cells (Fig. 2B), 51 and 62% in ST486 cells (Fig. 2C)
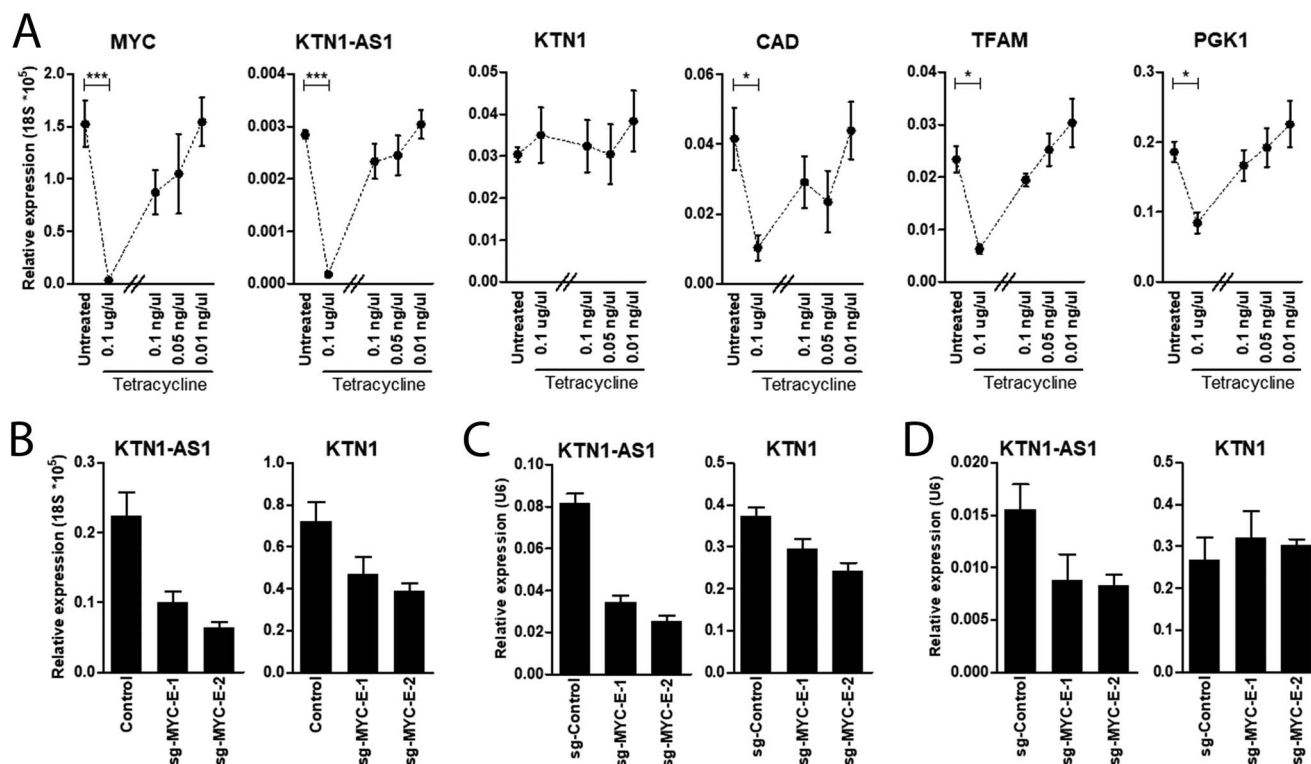
Figure 2. KTN1-AS1 is a direct target of MYC and dependent on the canonical Myc binding motif contained. (**A**) Gene expression changes after treatment of P493–6 cells with different concentrations of tetracycline, which cause a full or partial inhibition of Myc expression. CAD, TFAM and PGK1 are known targets of Myc. RT-qPCR, mean ± error, $n = 3$. Repeated measures ANOVA; * $P < 0.05$, *** $P < 0.001$. (**B**) Gene expression changes after treatment of Myc-on P493–6 cells with two sgRNAs designed to disrupt the Myc E-box binding motif or a non-targeting sgRNA (control). (**C**) ST486 and (**D**) CA46 cells treated with two E-box disrupting sgRNAs. Mean of two measurements at day 7 and day 11 post-infection is shown. RT-qPCR; mean ± SD.

and 40 and 22% in CA46 cells (Fig. 2D) in response to sg-MYC-E1 and sg-MYC-E2, respectively. As expected, KTN1 showed limited decreases in P493–6 (35 and 46%; Fig. 2B) and ST486 (14 and 30%; Fig. 2C) and no decrease in CA46 cells (Fig. 2D). Altogether, these data confirm that KTN1-AS1 is a direct target of Myc and that the induction of KTN1-AS1 by Myc is dependent on the integrity of the E-box binding motif.

To rule out a potential effect of KTN1-AS1 on the neighboring protein coding gene KTN1, we checked whether depletion of KTN1-AS1 affects KTN1 expression. KTN1-AS1 targeting shRNAs induced a >50 and ~30% reduction in transcript abundance in ST486 cells with shKTN1-AS1-1 and sh-KTN1-AS1-2, respectively (Supplementary Material, Fig. S3A). KTN1-AS1 knockdown had no effect on KTN1 mRNA levels (Supplementary Material, Fig. S3A). As expected, knockdown of KTN1 did not affect the expression levels of KTN1-AS1 (Supplementary Material, Fig. S3B). These data indicate that KTN1 and KTN1-AS1 do not influence each other at the transcriptional level.

KTN1-AS1 is overexpressed in multiple subtypes of lymphoma

To gain further insight into the deregulation of this lncRNA in lymphoma, we measured KTN1-AS1 as well as MYC transcript levels in a panel of lymphoma cell lines (Fig. 3A). MYC levels did not differ between normal B cell subsets but were significantly increased in Hodgkin lymphoma (HL; $P = 0.0059$), DLBCL ($P = 0.0005$) and BL ($P = 0.048$) cell lines compared with germinal center (GC-) B cells. KTN1-AS1 expression levels were slightly lower in GC-B cells compared with naïve and memory B cells. Similar to MYC, KTN1-AS1 levels were strongly increased in HL ($P = 0.034$), DLBCL ($P = 0.015$) and BL ($P = 0.005$) cell lines compared with GC-B cells. In addition, we analyzed frozen tissue samples of primary lymphoma including BL, CLL and DLBCL cases. Expression levels of both MYC ($P < 0.001$) and KTN1-AS1 ($P = 0.011$) were significantly higher in BL as compared with CLL (Fig. 3B). In primary DLBCL cases ($n = 299$) compared with normal GC-B cells (control; $n = 6$), MYC was significantly increased in ABC ($P = 0.0002$) but not GCB ($P = 0.063$) unclassified ($P = 0.059$) cases. Furthermore, MYC levels were significantly higher in ABC compared with GCB DLBCL cases ($P < 0.0001$), which is in line with the literature (6). KTN1-AS1 was significantly increased in all DLBCL subtypes compared with normal GC-B cells (ABC: $P < 0.0001$, GCB: $P = 0.0023$, unclassified: $P = 0.0009$). Like MYC, KTN1-AS1 levels were also more abundant in ABC compared with GCB DLBCL cases ($P < 0.0001$; Fig. 3C). These data are in line with KTN1-AS1 being a Myc-induced lncRNA and show that KTN1-AS1 is highly overexpressed in multiple lymphoma subtypes compared with their normal counterpart (i.e. GC-B cells).
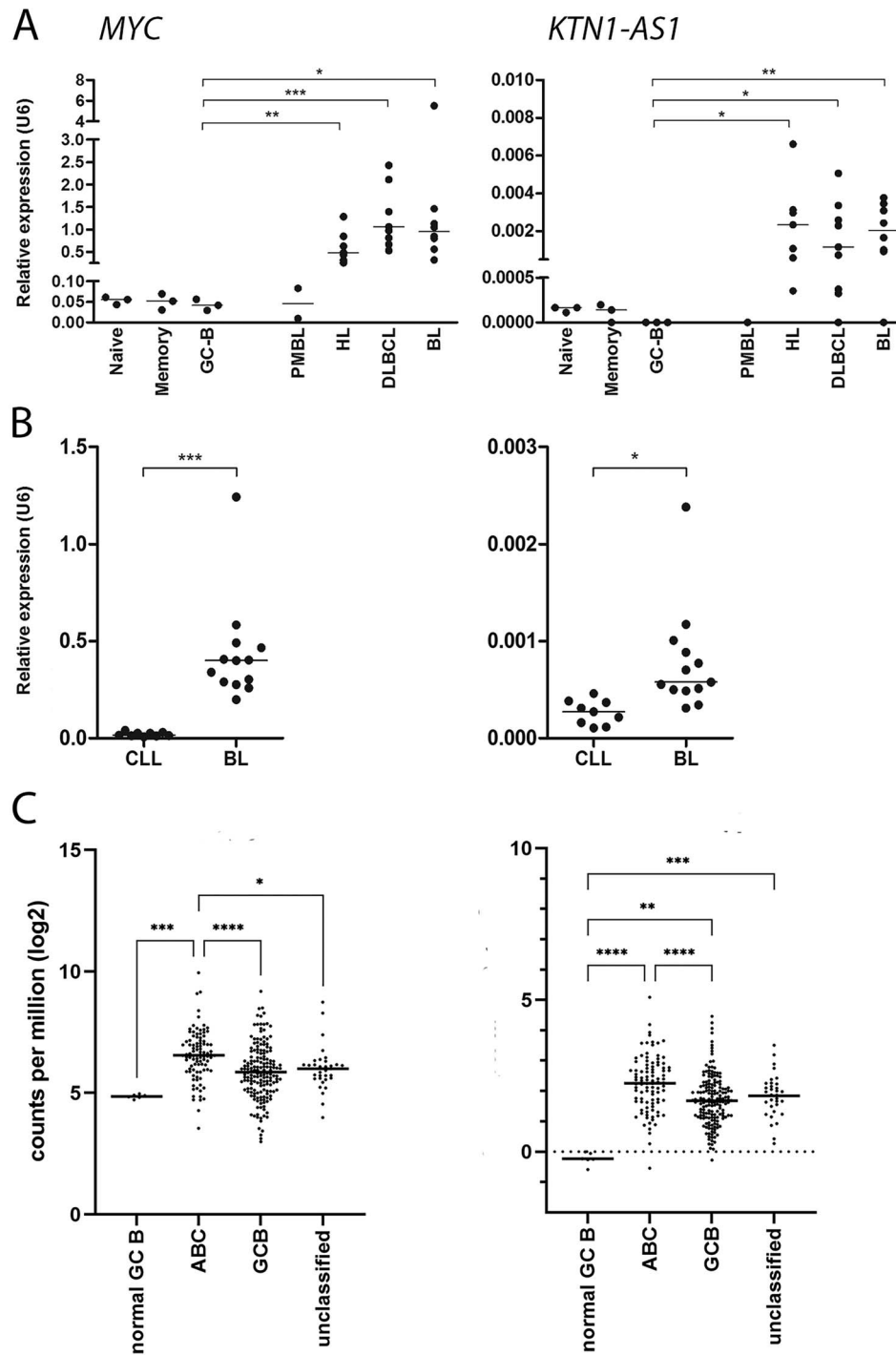
Figure 3. KTN1-AS1 is strongly overexpressed in multiple lymphoma subtypes with high MYC expression. (**A**) RT-qPCR expression analysis of MYC and KTN1-AS1 in sorted normal naïve, memory and germinal center (GC) B cell subsets ($n = 3$) and multiple lymphoma cell lines including primary mediastinal B-cell lymphoma (PMBL; $n = 2$), Hodgkin lymphoma (HL; $n = 7$), DLBCL ($n = 9$) and BL (BL; $n = 7$). RT-qPCR, mean ± error; t-test versus GC-B with Welch's correction. (**B**) RT-qPCR expression analysis in a set of fresh frozen tissue samples consisting of primary chronic lymphocytic leukemia (CLL; $n = 9$) characterized by low MYC levels and BL ($n = 13$) characterized by high MYC expression. RT-qPCR, mean ± error; t-test with Welch's correction. (**C**) RNA sequencing analysis of fresh frozen tissue samples of DLBCL and normal GC B cells isolated from tonsil. DLBCL cases were subclassified according to cell of origin into ABC ($n = 97$), GCG ($n = 169$) and unclassified ($n = 33$). Line indicates mean. Kruskal–Wallis and Dunn's multiple comparison test. * $P < 0.05$, ** $P < 0.01$, *** $P < 0.001$, **** $P < 0.0001$.

KTN1-AS1 depletion results in a strong growth decrease in BL

To establish the relevance of KTN1-AS1 for BL, we studied the effect of shRNA-mediated knockdown on growth.

shKTN1-AS1-1 caused a significant ($P < 0.0001$) growth decrease in three out of three and shKTN1-AS1-2 in two of three BL cell lines (Fig. 4A). A 50% decrease in GFP-positive cells was achieved at day 5, 15 and 20 after
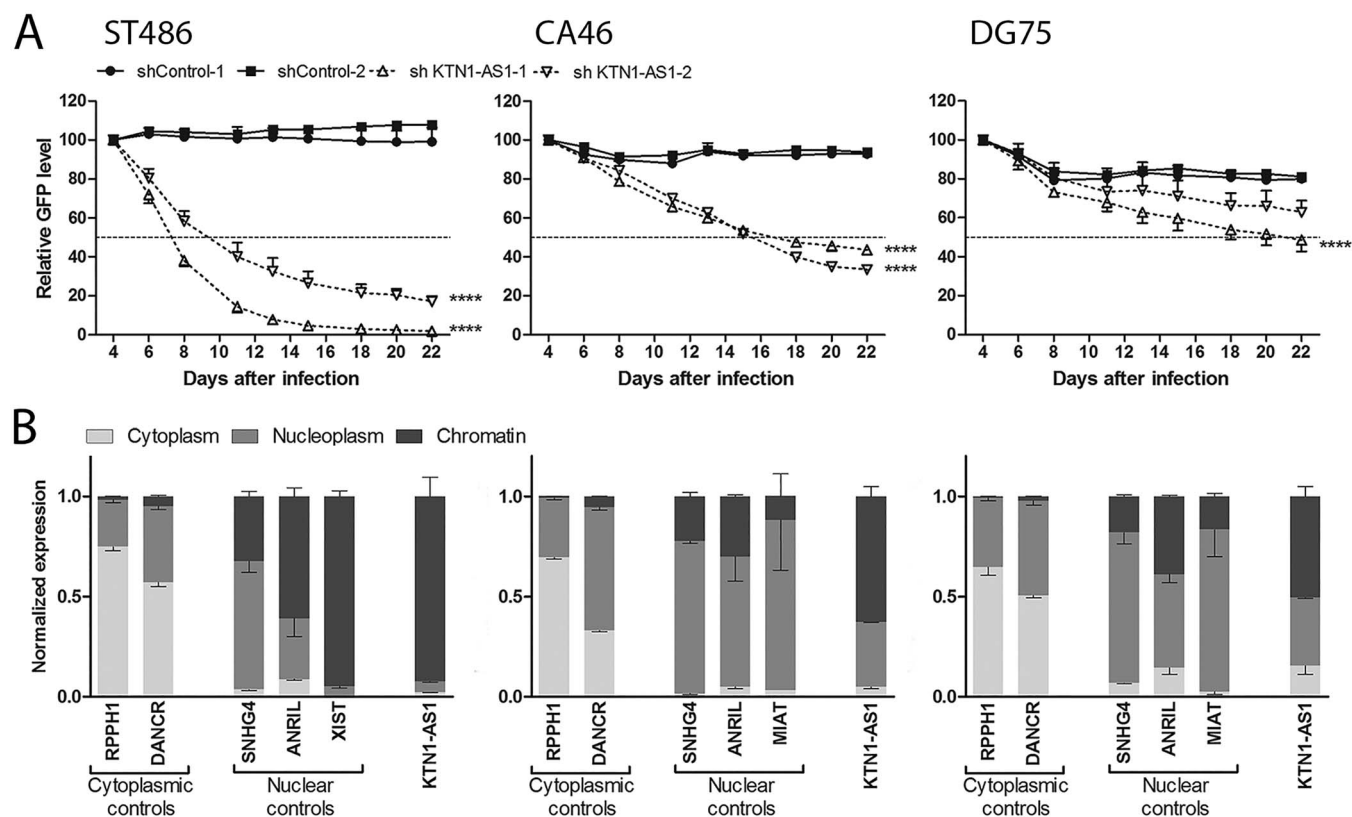
Figure 4. Depletion of nuclear lncRNA KTN1-AS1 causes a strong growth decrease in BL cells. (**A**) KTN1-AS1 depletion causes a strong growth decrease in three BL cell lines. GFP competition assay; mean ± SD, $n = 3$, **** $P < 0.0001$. (**B**) Subcellular fractionation was performed to study lncRNA localization in three BL cell lines. The indicated control lncRNAs confirm successful fractionation of cells. KTN1-AS1 shows strong nuclear localization. $N = 1$ per cell line.

infection with shKTN1-AS1-1 in ST486, CA46 and DG75 cells, respectively. For shKTN1-AS1-2, a 50% decrease was observed at day10 and 16 in ST486 and CA46, respectively. These results indicate a strong growth supportive role for KTN1-AS1 in BL.

To assess whether the decrease in GFP+ cells was due to the induction of caspase-mediated apoptosis, we first checked the levels of cleaved PARP. A minor increase of cleaved PARP levels was observed in ST486 for both KTN1-AS1 shRNAs (Supplementary Material, Fig. S4A). Next, we tested whether the caspase-inhibitor Q-VD could rescue the observed phenotype. Q-VD treatment caused a minor rescue of the growth reduction phenotype in ST486 cells infected with both KTN1-AS1 shRNAs (20 and 14%), although both control shRNAs also induced a minor effect in these cells (8 and 11%). In CA46 cells, a weak rescue was observed only for shKTN1-AS1-2 (14%), and no rescue was seen in DG75 cells (Supplementary Material, Fig. S4B). These data indicate that the growth decrease observed upon KTN1-AS1 depletion is for the largest part not due to the induction of caspase-mediated apoptosis.

KTN1-AS1 is a nuclear, chromatin-associated lncRNA

To gain insights into its function, we analyzed the abundance of KTN1-AS1 transcripts in cytoplasmic,

nucleoplasmic and chromatin fractions of three BL cell lines. Purity of the fractions was confirmed by the assessment of RNA transcripts with known subcellular localization: RPPH1 and DANCR as cytoplasmic, SNHG4, ANRIL and MIAT as nucleoplasmic and XIST (cell lines derived from female patients) as chromatin-associated transcripts (30,31). All control RNAs were enriched in the expected fractions in all cell lines (Fig. 4B). KTN1-AS1 were strongly enriched in the nuclear fractions (85–98% of KTN1-AS1 RNA), with preferential localization in the chromatin fractions (50–90% of KTN1-AS1 RNA) in all three cell lines. The nuclear localization of KTN1-AS1 supports a putative function in gene expression regulation.

Depletion of KTN1-AS1 has broad effects on gene expression in BL

We assessed genome-wide gene expression changes upon KTN1-AS1 depletion in ST486 cells, which is the cell line that had the strongest growth phenotype. By combining significant expression changes in KTN1-AS1-depleted cells harvested at day 4 and day 6 post-infection, we identified a total of 306 deregulated genes (260 coding and 46 noncoding; Supplementary Material, Table S2). Unsupervised hierarchical clustering of all responsive genes resulted in a clear separation between control and knockdown samples (Fig. 5A), and 44% of the deregulated

genes (133, of which 122 are coding) were increased in control versus knockdown samples (hereafter referred to as 'KTN1-AS1-induced'), while 56% (173, of which 138 are coding) were decreased ('KTN1-AS1-repressed'). Follow-up analyses were restricted to the protein coding genes affected by KTN1-AS1 knockdown.

To gain insight into the functional relevance of KTN1-AS1-dependent gene expression changes, we firstly performed GSEA. Multiple gene sets were positively correlated with KTN1-AS1-induced genes (i.e. were enriched in shControl-treated ST486 cells; Supplementary Material, Table S3), while no significant enrichments were detected for KTN1-AS1-repressed genes. We noted an enrichment of a Myc target gene set (Fig. 5B) that was also enriched in Myc-induced coding genes (Supplementary Material, Fig. S2A). A second Myc-related gene set generated in a murine p53^{null}/MYC^{high} B cell lymphoma model showed opposite regulation (YU_MYC_TARGETS_DN) (32). Other notable enrichments include genes upregulated in CLL with poor prognosis (as characterized by VH3–21 expression [FAELT_B_CLL_WITH_VH3_21_UP] (33) or high levels of ZAP70/CD38 [HUTTMANN_B_CLL_POOR_SURVIVAL_UP] (34)) as well as genes responding to serum stimulation (with or without contribution of MYC) in P493-6 cells (SCHLOSSER_SERUM_RESPONSE_UP, SCHLOSSER_SERUM_RESPONSE_AUGMENTED_BY_MYC) (35). Second, we performed Enrichr analysis on the defined sets of KTN1-AS1-induced ($n = 122$) and KTN1-AS1-repressed ($n = 138$) coding genes. This revealed a highly significant enrichment of genes involved in cholesterol biosynthesis according to the Reactome_2016 (5 of 23 genes; adj. $P = 0.0001$), GO_Biological_Process (6 of 59 genes; adj. $P < 0.001$) and KEGG_2016 (3 of 20 genes, adj. $P = 0.019$) databases (Supplementary Material, Table S4). This included essential enzymes at almost every step of the biosynthesis pathway (Supplementary Material, Fig. S5A). Moreover, we again observed enrichment for genes that have TF binding sites for MYC and/or its cofactor MAX within KTN1-AS1-induced genes (adj. $P = 0.005$ for both; Supplementary Material, Table S4). In line with this, four of the six cholesterol pathway genes reduced upon KTN1-AS1 knockdown were also significantly reduced upon MYC knockdown (i.e. ACLY, FDPS, DHCR7, DHCR24; Supplementary Material, Fig. S5B). KTN1-AS1-repressed genes were associated with Glycosphingolipid biosynthesis and binding of *Interferon Regulatory Factor 8* (IRF8), a co-regulator of IFN-γ response genes. Altogether, these data suggest that the upregulation of KTN1-AS1 in BL affects a wide array of genes involved in proliferation and co-regulates many MYC target genes.

KTN1-AS1 potently co-regulates MYC-target genes

To further investigate gene co-regulation of KTN1-AS1 and Myc, we assessed what proportion of KTN1-AS1 regulated genes are also bound by Myc. We found that 42% of the KTN1-AS1-regulated loci were bound by Myc in five BL cell lines, of which 7% possessed a Myc E-Box (Fig. 5A; Supplementary Material, Table S2). This was especially apparent within KTN1-AS1-induced genes (58% Myc-bound, 13% with E-Box) and very similar to what we observed for Myc-regulated loci (57% Myc-bound, 13% with E-Box; Supplementary Material, Fig. S2B). We therefore investigated whether KTN1-AS1 knockdown influences MYC expression. Although two microarray probes against MYC were not in our final list of KTN1-AS1 regulated genes, we did detect substantial decreases of both *MYC* mRNA (Fig. 5C) and Myc protein (Fig. 5D) upon knockdown of KTN1-AS1 in ST486 cells. The strength of this effect correlated with the KTN1-AS1 knockdown efficacy, which was slightly higher for shKTN1-AS1-1 compared with shKTN1-AS1-2 (causing ∼55% MYC/46% Myc and ∼30% MYC/21% Myc reductions, respectively). CA46 cells showed minor decreases in *MYC* mRNA and protein (∼20% MYC/16% Myc and ∼15% MYC/9% Myc reductions). Furthermore, we observed strong similarities in expression patterns between KTN1-AS1-regulated genes in ST486 cells and the earlier defined Myc-regulated genes in ST486 and P493-6 cells (Supplementary Material, Fig. S5C; Supplementary Material, Table S2). These data suggest that KTN1-AS1 is an important co-regulator for a variety of genes regulated by Myc and may, in some cell lines, also affect the transcriptional levels of Myc itself.

Discussion

In this study, we identified the lncRNA KTN1-AS1 as a direct target of the oncogenic transcription factor Myc in BL cells. We showed that KTN1-AS1 is strongly overexpressed in multiple Myc-positive lymphoma subtypes, including BL, HL and DLBCL. In addition, we showed that its downregulation has profound effects on BL cell growth. This effect is likely mediated via potent co-regulation of a variety of Myc-target genes, including essential genes in cholesterol synthesis.

The intersection of four datasets applied here produced a comprehensive list of Myc-induced protein coding genes of which many were previously defined as Myc-targets. The lack of enrichment of Myc-binding and E-box sequences in Myc-repressed genes is in line with the idea that these changes are the result of the decreases in overall RNA levels rather than a direct effect induced by Myc (36,37). As mRNAs and lncRNAs are subject to the same regulatory mechanisms (38), our approach was suitable to identify direct lncRNA targets of Myc. The relevance of MYC as a regulator of KTN1-AS1 was supported by the highly similar expression patterns in primary lymphoma samples and the effect of MYC repression on KTN1-AS1 expression in the P493-6 model. Furthermore, CRISPR/Cas9 experiments showed that the integrity of the Myc E-Box is essential for the induction of KTN1-AS1. We did not observe strict linear correlations between Myc and KTN1-AS1 in either cell lines or patient cases. KTN1-AS1 is thus most likely co-regulated by additional factors
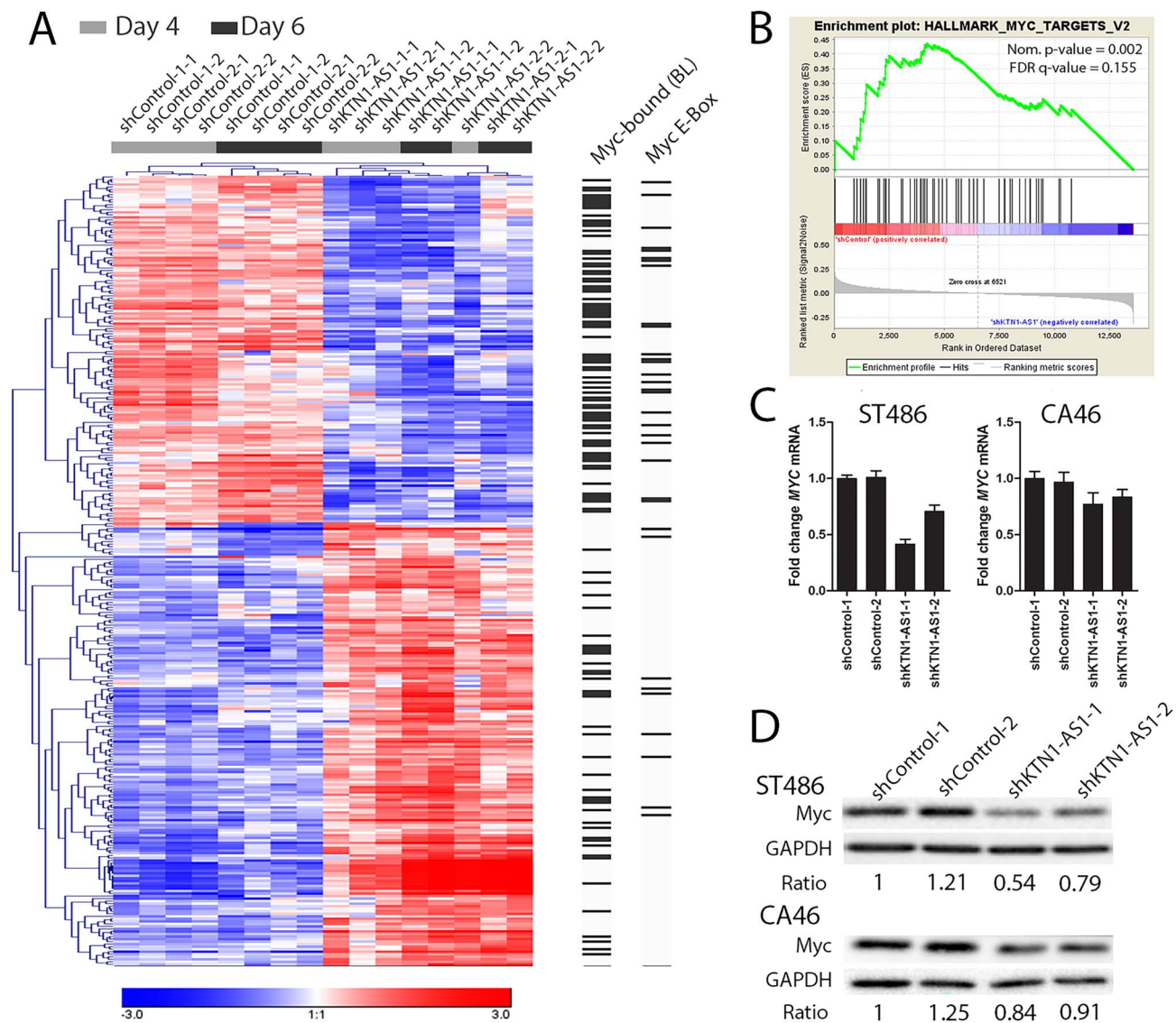
Figure 5. KTN1-AS1 affects Myc levels and Myc target genes. (**A**) Gene expression changes observed 4 and 6 days after KTN1-AS1 depletion in ST486 cells; 312 deregulated probes are shown (137 induced, 175 repressed); unsupervised hierarchical clustering with Pearson correlation. On the right is indicated which of the KTN1-AS1 responsive probes are bound by Myc in five BL cell lines (ChIP) and/or have a canonical Myc E-Box (GSEA). (**B**) Myc-related gene set enriched in KTN1-AS1 affected genes. GSEA; $P = 0.002$; FDR = 0.15. (**C**) Two BL cell lines show a reduction of Myc mRNA upon KTN1-AS1 depletion. RT-qPCR; mean of two replicates harvested at day 4 after shRNA infection. (**D**) Decrease in Myc protein after KTN1-AS1 depletion day 6 after shRNA infection. A representative blot of three replicates is shown.

as is also known for MYC (22). In line with this, a plethora of TF binding sites is present in the promoter region of KTN1-AS1 (GENCODE; GM12878 lymphoblastoid cells), including cancer growth-related activators (e.g. STAT1) and repressors (e.g. RB1).

In colorectal and prostate cancer cells, KTN1-AS1 ('MycLo-3') was shown to have a function in cell cycle regulation, with its depletion causing deregulation of 13 cell cycle-related genes and an increase in S/G2-phase cells (39). In BL cells, only two (i.e. MCM4, ARF3) of these 13 putative KTN1-AS1-target genes showed expression changes. GSEA analysis revealed an association of high KTN1-AS1 levels with G2/M checkpoint genes (BIOCARTA_G2_PATHWAY, 24 genes); however, this reflects only minor expression changes

(FC < 1.5) as none of these were included in our final list of KTN1-AS1 regulated genes. Accordingly, we did not observe any changes in cell cycle distribution upon KTN1-AS1 depletion (data not shown). KTN1-AS1 has furthermore been suggested to act as a sponge for multiple micro RNAs, including miR-23b (non-small cell lung cancer, pancreatic cancer) (40,41), miR-23c (hepatocellular carcinoma) (40), miR-130a (squamous cell carcinoma) (42), miR-153 (43) and miR-505 (glioma) (44). Although several of these miRNAs are expressed in BL, we did not observe enrichment of KTN1-AS1 in any of the Ago2-IP experiments conducted in five different BL cell lines (unpublished observations). We previously identified the miR-150 sponging transcripts ZDHHC11 and ZDHHC11B using Ago2-IP in BL cells (45), showing

that miRNA sponges are present in the RISC complex and can be identified using this method. In bladder cancer, KTN1-AS1 was suggested to activate KTN1 in *cis* via recruitment of the histone acetylase p300 (46). The authors observed significant KTN1 expression changes upon transfection of KTN1-AS1 targeting shRNAs in two bladder cancer cell lines (46), an effect we did not observe in the three BL cell lines tested. Across 299 DLBCL patient cases, there was no significant positive correlation of KTN1 and KTN1-AS1 expression ($R^2 = 0.134$). The role of KTN1-AS1 in B-cell lymphoma is likely different from the functions described in these cancer types.

Other Myc-regulated lncRNAs have been described to promote *MYC* expression at the transcriptional (CCAT-2, PCGEM1) (47,48) or post-transcriptional level (MIF, GHET1, XLOC_010588, PCAT-1, RoR, FGF13-AS1, MTSS1-AS) in cell-type specific manner (12,49–54). The chromatin-association of KTN1-AS1 as well as the observed effect on both *MYC* mRNA and Myc protein levels upon KTN1-AS1 depletion in ST486 cells suggest a transcriptional mechanism. No sequence similarities were found between KTN1-AS1 and *MYC* or its promoter region, which makes regulation through base-pairing unlikely. Alternatively, KTN1-AS1 could act as a co-factor for MYC-dependent transcriptional regulation of MYC-target genes (i.e. including *MYC* itself). Lastly, we cannot exclude the possibility that the downregulation of MYC upon KTN1-AS1 knockdown is a secondary effect of decreased cell proliferation.

A prevalent effect observed upon KTN1-AS1 depletion in BL cells was the downregulation of six major enzymes in the cholesterol biosynthesis pathway. Only four of these six cholesterol pathway genes were also significantly affected by MYC knockdown, making it partially specific to KTN1-AS1. MYC has previously been shown to directly activate other important cholesterol pathway genes (i.e. ACACA, HMGCR) in P493-6 and lymphoblastoid GM12878 cells (55). We confirm this observation for ACACA, which showed a 1.8 and 4.2-fold increase in ST486 and P493-6 cells in their MYC-high versus MYC-low states, respectively. Our data thus suggest that MYC and KTN1-AS1 cooperate in the activation of key cholesterol pathway genes. Cholesterol is required for the assembly of lipid rafts in the cell membrane, which in turn are essential for signal transduction. Depletion of cholesterol biosynthesis can thereby hamper proliferation-associated stimuli through, e.g. the B cell receptor, Akt and interferons (56–58). In line with this, targeting of cholesterol and lipid rafts was shown to mediate significant anti-tumor activity in lymphomas (59,60). Conversely, the anti-tumor effect of Rituximab, depending on CD20 receptor activation, is strongly decreased by low levels of cholesterol in the cell membrane (57).

To conclude, we defined KTN1-AS1 as a Myc-induced lncRNA with major regulatory effects on cancer related pathways in BL, influencing Myc signaling and co-regulating cholesterol biosynthesis. Therefore, KTN1-AS1 qualifies as an oncogenic factor and represents a putative novel therapeutic target in lymphoma.

Materials and Methods
Cell culture, cell line panel and treatments

BL cell lines were purchased from ATCC (ST486) and DSMZ (CA46 and DG75); P493-6 B cells were a kind gift of Prof. D. Eick (Helmholtz center Munich). Cell lines were cultured at 37°C under an atmosphere containing 5% CO2 in RPMI-1640 medium supplemented with 2 mM ultra-glutamine, 100 U/mL penicillin, 0.1 mg/mL streptomycin and 20% (ST486) or 10% (P493-6, CA46 and DG75) fetal calf serum (all reagents from Cambrex Biosciences, Walkersville, MD, USA). At regular intervals, cell lines were tested for mycoplasma contamination by PCR (61) and subjected to short tandem repeat genotyping using the PowerPlex 16HS system (Promega, Madison, WI, USA) to confirm cell line identity. The cell lines included in the panel were purchased from DSMZ, cultured according to their proposed culture conditions and included: PMBL—Primary mediastinal B-cell lymphoma (K1106P, MedB1); HL—Hodgkin lymphoma (L428, L540, L1236, KM-H2, SUP-HD1, DEV), DLBCL (SUDHL-2, −4 to −6 and −10, SC-1, OCILy3, U2932, DOHH2) and BL (ST486, CA46, DG75, RAMOS, BL65, Namalwa, Raji, Jijoye).

Q-VD-Oph (Cat# S7311; Selleckchem, Munich, Germany) stock of 5 mM dissolved in 100% DMSO was used to inhibit caspase activity. Medium was supplemented with Q-VD (10uM) or DMSO starting 24 h after lentiviral infection and on every following culture day.

Patient samples and normal B cell subsets

Frozen tissue sections of 13 BL (MYC translocation, EBV⁻, CD20⁺, CD10⁺ and BCL2⁻) and 9 primary lymph node derived CLL (CD20⁺, CD5⁺, cyclin D1⁻ and variable ZAP-70 expression) cases used for RT-qPCR analysis were described previously (15). Each individual diagnosis was reviewed by an experienced hematopathologist according to the World Health Organization classification (62). All protocols for obtaining human tissue samples were performed in accordance with the guidelines from the Institutional Review Board or Medical Ethical Committee of the University Medical Center Groningen (UMCG).

Frozen tissue sections from 299 DLBCL patients were collected at the BC Cancer Center Vancouver and subjected to RNA sequencing as described previously (63). DLBCL cases were subclassified according to Lymph2Cx cell of origin classifier (64) into ABC ($n = 97$), GCB ($n = 169$) and unclassified ($n = 33$). The raw sequencing data have been deposited in the European Genome-phenome Archive (EGA) under accession number EGAS00001002657 (Dataset EGAD00001003783). Three sets of GC B-cells isolated from tonsillectomies were used as normal controls. Normal B-cell subsets were sorted by FACS from three different tonsil samples as described previously (65) and included naive B cells (CD19⁺ IgD⁺, CD38⁻), GC B cells (CD19⁺ IgD⁻, CD38⁺)

and memory B cells (CD19$^+$ IgD$^-$, CD38$^-$). Written permission for the use of the tonsil tissues to isolate GC B-cells was obtained from the parents of the children. The study protocol was consistent with international ethical guidelines (the Declaration of Helsinki and the International Conference on Harmonization Guidelines for Good Clinical Practice).

Subcellular fractionations

Cytoplasmic, nuclear and chromatin fractions of BL cell lines were separated as described previously (66) with some modifications. In brief, cell pellets were lysed on ice in 1× lysis buffer (10 mM Tris–HCL pH 8, 300 mM sucrose, 10 mM NaCl, 2 mM MgAc2, 3 mM CaCl2, 0.1% Nonidet P-40, 0.5 mM DTT) and centrifuged at 1.000×g for 5 min at 4°C to yield the cytoplasmic fraction. The nuclei fraction was washed once in glycerol buffer (50 mM Tris–HCL pH 8.0, 25% glycerol, 5 mM MgAc2, 0.1 mM EDTA, 5 mM DTT). To separate nucleoplasmic and chromatin fractions, nuclei were lysed in Urea Buffer (20 mM HEPES pH 7.5, 7.5 mM MgCl2, 0.1 mM EGTA, 0.3 M NaCl, 1 M Urea, 1% Nonidet P-40, 1 mM DTT) and centrifuged at 14.000×g for 10 min at 4°C. All buffers were supplemented with 20u/mL RNAseOUT and 1× Complete™ EDTA-free protease inhibitor cocktail (Roche Penzberg, Germany) prior to use. Qiazol lysis reagent (Qiagen, Hilden, Germany) was added to all fractions for RNA isolation.

shRNA-mediated knockdown

ShRNAs were designed using the Invivogen siRNA wizard and sense (S) and antisense (AS) oligo's (Supplementary Material, Table S1) were ordered from Integrated DNA Technologies (IDT, Coralville, Iowa, USA) and cloned into the pGreenpuro lentiviral vector (SBI, MountainView, CA, USA). Generation of viral particles and infection of cells was performed as described previously (15). Flow cytometry was used to assess the percentage of infected cells based on GFP expression. Cells were harvested directly if GFP+ cells were >90% or after sorting GFP+ cells at day 4 and day 6 (KTN1 and KTN1-AS1 knockdown) or day 8 (MYC knockdown) after infection.

Western blotting

Cells were washed with cold PBS and lysed either in Lysis Buffer (#9803, Cell Signaling Technology, Danvers, MA, United States) (BL cell lines, MYC knockdown samples) or in RIPA buffer (50 mM Tris, 150 mM NaCl, 2,5 mM Na2EDTA, 1% Triton X-100, 0.5%mM sodium deoxycholate, 0.1% SDS) (all other samples) with 1 mM phenylmethanesulphonyl fluoride for 45 min on ice. Subcellular fractionation samples (cytoplasm, nucleoplasm) were used in their respective lysis buffers. Lysates were cleared by centrifugation (14 000×g, 10 min, 4°C) and protein concentrations were determined using Pierce BCA Protein Assay (Thermo scientific, Rockford, IL, USA) according to the manufacturer's instructions, and 10% polyacrylamide gels were used for separation followed by transfer onto nitrocellulose membranes

using standard procedures. Membranes were blocked in 5% milk supplemented with Tris-buffered saline and 0.1% Tween-20 followed by incubation overnight at 4°C with the following antibodies: rabbit monoclonal anti-human Myc antibody (Y69) (Cat# 1472–1, Epitomics, Burlingame, USA); rabbit monoclonal anti-human Myc antibody (Y69) (Cat# ab32072; Abcam, Cambridge, UK); rabbit polyclonal anti-human (cleaved) PARP (Cat# 9542; Cell Signaling, Danvers, MA, USA); Polyclonal horseradish peroxidase–conjugated goat anti-rabbit Ig (1000×) and rabbit anti-mouse Ig (1000×; both from Dako, Glostrup, Denmark) were used as secondary antibodies. Membranes were incubated with Super Signal West Pico Chemiluminescent Substrate (Thermo Scientific) according to the manufacturer's instructions and signals were visualized on the ChemiDoc MP scanner (Bio-Rad, Veenendaal, The Netherlands). Image Lab 4.0.1 Software (Bio-Rad, Veenendaal, The Netherlands) was used for quantification of protein bands.

GFP competition assays

GFP measurements were performed tri-weekly for a period of 3 weeks starting at day 4 after infection. The relative number of GFP+ cells was calculated by normalization to the first measurement (range 20–60% GFP+ cells). All GFP competition assays were performed in triplicate per shRNA and per cell line. Non-targeting control shRNAs were included in all experiments.

Microarray analysis

Two array designs were used in this study. MYC knockdown samples were hybridized to a custom design lncRNA/mRNA array ('Custom array', AMADID: 039731). Array design and procedures were described previously (15). KTN1-AS1 knockdown samples were hybridized to a commercially available microarray ('Agilent array', AMADID: 072363; Agilent Technologies, Santa Clara, CA, USA) following the same procedures. The Custom and Agilent arrays contained 26 426 and 33 680 probes against coding and 31 054 and 19 049 probes against noncoding transcripts, respectively, and 29 779 probes are shared between both arrays, which includes most protein coding genes probes.

Raw data were extracted with Agilent Feature Extraction software v12 and analyzed with Genespring GX 13.1.1 software (Agilent Technologies). Probes flagged as present by the feature extracting software and consistently expressed in the 10th to 100th percentile in at least 1 out of 2 conditions (i.e. knockdown or control) were used for further analysis. Using these settings, 7192 lncRNA probes and 13 741 mRNA probes (5040 and 10 670 loci) were expressed above background in ST486 cells with Myc knockdown, and 3012 lncRNA and 14 760 mRNA probes (2425 and 11 368 loci) in ST486 cells with KTN1-AS1 knockdown. LncRNA probes with high similarity to coding genes and probes detecting pseudogenes were excluded from the final lists of differentially expressed lncRNA transcripts.

Heatmaps were generated with Genesis software v1.8.1 (67) (Institute for Genomics and Bioinformatics Graz, Graz, Austria) using unsupervised hierarchical clustering with Pearson correlation as the distance metric. Microarray data are available at the Gene Expression Omnibus (GEO) database (GSE119925).

Enrichment analysis
GSEA was performed using the Hallmarks gene sets of the Molecular Signatures Database (http://www.broad.mit.edu/gsea) (68,69) on all coding probes expressed above background for MYC and KTN1-AS1 shRNA treated ST486 cells. Nominal *P*-values (i.e. significance of a single gene set's enrichment score based on the permutation-generated null distribution) and FDR *q*-values (multiple testing correction applied) are reported as measure of significance. Enricher (http://amp.pharm.mssm.edu/Enrichr/) (70,71) was used to assess transcription factor binding site (ENCODE/CHEA TFs dataset) and pathway (KEGG, Reactome) enrichment.

Myc binding site and E-box analysis
To select for well-annotated genes, only probes mapping to either RefSeq genes or annotated lincRNAs (2) were considered for Myc binding site analysis (52 728 and 57 480 probes on Agilent and Custom arrays, respectively). ChIP data were retrieved from Seitz *et al.* (25) (Myc binding sites in BL cell lines). For all transcripts with a probe on the microarray, the TSS was determined and the presence of a Myc-binding site ±5 kb was assessed using Galaxy (72,73).

GSEA was employed to determine which coding gene loci possess Myc E-box motifs in close vicinity (i.e. ±2 kb) of their transcriptional start sites. Seven gene sets assign the canonical Myc binding motif CACGTG (CACGTG_MYC_Q2, MYC_Q2, BENPORATH_MYC_TARGETS_WITH_EBOX) or NNAC**CACGTG**GT NN (MYCMAX_01, MYCMAX_02, MYCMAX_03, MYCMAX_B) to specific genes. These lists were overlapped with our set of Myc-responsive genes. For lncRNAs that fulfilled the criteria of being Myc-responsive in ST486 and P493-6 cells and bound by Myc in BL cells ($n = 7$), the region ±5 kb of the TSS was manually scanned for the presence of canonical (CACGTG) and non-canonical (CATGTG, CACGCG, CGCGTG, CACGAG, CATGCG, CACGTT) E-box motifs.

RNA isolation and quantitative (q)RT-PCR
RNA isolation from cell lines and normal B cells was performed using Phase Lock Gel Heavy tubes (5 Prime Inc., Hilden, Germany) in combination with the miRNeasy mini/micro kit (Qiagen) according to the manufacturer's instructions. RNA from FFPE tissue sections was isolated using the RNeasy FFPE kit (Qiagen). On-column DNAse digestion was performed for all samples. RNA concentration was measured with a NanoDropTM 1000 Spectrophotometer (Thermo Fisher Scientific Inc., Waltham, USA); RNA integrity was

assessed on a 1% agarose gel. cDNA was synthesized using random primers, dNTP mix and the Superscript II Reverse Transcriptase Kit (Life Technologies Europe BV, Bleiswijk, NL) according to manufacturer's instructions. An input of 500 ng RNA was used per sample in a total reaction volume of 20 μL.

To detect transcript levels, SYBRgreen mix (Applied Biosystems B.V., Bleiswijk, The Netherlands) was used in a qPCR reaction volume of 10 μL with 1 ng cDNA and 150–300 nM primers in on a Lightcycler 480 system (Roche, Penzberg, Germany). Primer sequences used in this study are listed in Supplementary Material, Table S1. Relative expression levels are calculated based on the expression of the housekeeping genes TBP or U6. TBP was generally used for normalization in BL cell line experiments. U6 was the most stable housekeeping gene (of 10 tested) in highly heterogeneous sample populations including the cell line panel and primary patient cases.

CRISPR/Cas9 disruption of KTN1-AS1 E-box motif
Two sgRNAs targeting the E-box in KTN1-AS1 gene were designed using CRISPOR tool (74) and two control non-targeting sgRNAs were used from the Brunello library (75) (Supplementary Material, Table S1). Sense and antisense oligos were ordered from Genomed, Poland, annealed and cloned into the lentiCRISPR_v2 vector (a gift from Feng Zhang, Addgene plasmid #52961) (76). Lentiviral particles containing individual constructs were produced in HEK293T cells using the second generation packaging system. CA46, ST486 and P493-6 cells were transduced by spinfection (1000 g, 2 h, 33°C), and 24 h after transduction virus containing medium was removed and cells were plated in fresh medium with addition of puromycin for selection of successfully transduced cells (2.5 μg/ml for CA46; 0.3 μg/ml for ST486; 1 μg/ml for P493-6). Cells were selected with puromycin for 4 days and collected for DNA and RNA isolation at day 7 and/or 11 after transduction. To determine the efficiency of genome editing, a genomic region of ca. 800 bp flanking the E-box was amplified from wild type cells and cells transduced with E-box targeting sgRNAs using primers KTN1-AS1-Ebox_F and KTN1-AS1-Ebox_R. PCR products were Sanger sequenced using the same primers at Genomed, Poland. Based on sequencing results, TIDE analysis (29) was performed to determine the efficiency of E-box disruption and spectrum of introduced mutations.

Statistics
For GFP competition assays, the significance of changes in GFP+ cell percentages in knockdown samples compared with controls was assessed as described previously using a mixed model analysis (77). Differences in GFP+ cell percentages upon DMSO or Q-VD treatment were determined using repeated measures ANOVA and Tukey's Multiple comparison test, comparing DMSO and Q-VD per shRNA construct. Probes significantly differential expressed between knockdown and control conditions were determined using a moderated T test

(P-value cutoff: 0.05) and Benjamini–Hochberg multiple testing correction, followed by selection of probes with a >1.5-fold change in expression. For comparison, previously published microarray data from P493-6 cells (15) (GSE59480) were reanalyzed using the same settings and a >2-fold change in expression cutoff (conditions: MycOFF versus MycON all time points; MycOFF versus MycON-4 h). Enrichment of binding sites or CpG islands was evaluated using chi-square test. The percentages of probes with a specific feature within all probes deregulated upon Myc or KTN1-AS1 knockdown were compared with the percentages of probes with the same feature within all probes present on the array. Significant expression differences for the qPCR data for the cell line panel and BL versus CLL patient cases were tested using standard T test with Welch's correction (naive, memory, PMBL, HL, DLBCL or BL versus GC B; BL versus CLL). Significant differences between normal GC B cells and DLBCL patient cases grouped as GCB, ABC and unclassified were calculated using a Kruskal–Wallis test with Dunn's multiple comparison correction.

Supplementary Material

Supplementary Material is available at HMG online.

References

1. Derrien, T., Johnson, R., Bussotti, G., Tanzer, A., Djebali, S., Tilgner, H., Guernec, G., Martin, D., Merkel, A., Knowles, D.G. *et al.* (2012) The GENCODE v7 catalog of human long noncoding RNAs: analysis of their gene structure, evolution, and expression. *Genome Res.*, **22**, 1775–1789.
2. Cabili, M.N., Trapnell, C., Goff, L., Koziol, M., Tazon-Vega, B., Regev, A. and Rinn, J.L. (2011) Integrative annotation of human large intergenic noncoding RNAs reveals global properties and specific subclasses. *Genes Dev.*, **25**, 1915–1927.
3. Leucci, E., Vendramin, R., Spinazzi, M., Laurette, P., Fiers, M., Wouters, J., Radaelli, E., Eyckerman, S., Leonelli, C., Vanderheyden, K. *et al.* (2016) Melanoma addiction to the long non-coding RNA SAMMSON. *Nature*, **531**, 518–522.
4. Karube, K. and Campo, E. (2015) MYC alterations in diffuse large B-cell lymphomas. *Semin. Hematol.*, **52**, 97–106.
5. Korac, P., Dotlic, S., Matulic, M., Zajc, P.M. and Dominis, M. (2017) Role of MYC in B cell lymphomagenesis. *Genes (Basel)*, **8**, 115.
6. Hu, S., Xu-Monette, Z.Y., Tzankov, A., Green, T., Wu, L., Balasubramanyam, A., Liu, W., Visco, C., Li, Y., Miranda, R.N. *et al.* (2013) MYC/BCL2 protein coexpression contributes to the inferior survival of activated B-cell subtype of diffuse large B-cell lymphoma and demonstrates high-risk gene expression signatures: a report from the international DLBCL rituximab-CHOP consortium program. *Blood*, **121**, 4021.
7. Nguyen, L., Papenhausen, P. and Shao, H. (2017) The role of c-MYC in B-cell lymphomas: diagnostic and molecular aspects. *Genes (Basel)*, **8**, 116.
8. Fernandez, P.C., Frank, S.R., Wang, L., Schroeder, M., Liu, S., Greene, J., Cocito, A. and Amati, B. (2003) Genomic targets of the human c-myc protein. *Genes Dev.*, **17**, 1115–1129.
9. Benetatos, L., Benetatou, A. and Vartholomatos, G. (2020) Long non-coding RNAs and MYC association in hematological malignancies. *Ann. Hematol.*, **99**, 2231–2242.
10. Feng, Y.C., Liu, X.Y., Teng, L., Ji, Q., Wu, Y., Li, J.M., Gao, W., Zhang, Y.Y., La, T., Tabatabaee, H. *et al.* (2020) C-myc inactivation of p53 through the pan-cancer lncRNA MILIP drives cancer pathogenesis. *Nat. Commun.*, **11**, 4980-020-18735-8.
11. Hua, Q., Jin, M., Mi, B., Xu, F., Li, T., Zhao, L., Liu, J. and Huang, G. (2019) LINC01123, a c-myc-activated long non-coding RNA, promotes proliferation and aerobic glycolysis of non-small cell lung cancer through miR-199a-5p/c-myc axis. *J. Hematol. Oncol.*, **12**, 91.
12. Ma, F., Liu, X., Zhou, S., Li, W., Liu, C., Chadwick, M. and Qian, C. (2019) Long non-coding RNA FGF13-AS1 inhibits glycolysis and stemness properties of breast cancer cells through FGF13-AS1/IGF2BPs/Myc feedback loop. *Cancer Lett.*, **450**, 63–75.
13. Doose, G., Haake, A., Bernhart, S.H., Lopez, C., Duggimpudi, S., Wojciech, F., Bergmann, A.K., Borkhardt, A., Burkhardt, B., Claviez, A. *et al.* (2015) MINCR is a MYC-induced lncRNA able to modulate MYC's transcriptional network in burkitt lymphoma cells. *Proc. Natl. Acad. Sci. U. S. A.*, **112**, E5261–E5270.
14. Hart, J.R., Roberts, T.C., Weinberg, M.S., Morris, K.V. and Vogt, P.K. (2014) MYC regulates the non-coding transcriptome. *Oncotarget*, **5**, 12543–12554.
15. Winkle, M., van den Berg, A., Tayari, M., Sietzema, J., Terpstra, M., Kortman, G., de Jong, D., Visser, L., Diepstra, A., Kok, K. *et al.* (2015) Long noncoding RNAs as a novel component of the myc transcriptional network. *FASEB J.*, **29**, 2338–2346.
16. Kajino, T., Shimamura, T., Gong, S., Yanagisawa, K., Ida, L., Nakatochi, M., Griesing, S., Shimada, Y., Kano, K., Suzuki, M. *et al.* (2019) Divergent lncRNA MYMLR regulates MYC by eliciting DNA looping and promoter-enhancer interaction. *EMBO J.*, **38**, e98441.
17. Olivero, C.E., Martínez-Terroba, E., Zimmer, J., Liao, C., Tesfaye, E., Hooshdaran, N., Schofield, J.A., Bendor, J., Fang, D., Simon, M.D. *et al.* (2020) p53 activates the long noncoding RNA Pvt1b to inhibit myc and suppress tumorigenesis. *Mol. Cell*, **77**, 761–774.e8.
18. Chen, B., Dragomir, M.P., Fabris, L., Bayraktar, R., Knutsen, E., Liu, X., Tang, C., Li, Y., Shimura, T., Ivkovic, T.C. *et al.* (2020) The long noncoding RNA CCAT2 induces chromosomal instability through BOP1-AURKB signaling. *Gastroenterology*, **159**, 2146–2162.e33.
19. Shigeyasu, K., Toden, S., Ozawa, T., Matsuyama, T., Nagasaka, T., Ishikawa, T., Sahoo, D., Ghosh, P., Uetake, H., Fujiwara, T. *et al.* (2020) The PVT1 lncRNA is a novel epigenetic enhancer of MYC, and a promising risk-stratification biomarker in colorectal cancer. *Mol. Cancer*, **19**, 155-020-01277-4.
20. Wang, Z., Yang, B., Zhang, M., Guo, W., Wu, Z., Wang, Y., Jia, L., Li, S., Cancer Genome Atlas Research Network, Xie, W. *et al.* (2018) lncRNA epigenetic landscape analysis identifies EPIC1 as an oncogenic lncRNA that interacts with MYC and promotes cell-cycle progression in cancer. *Cancer Cell*, **33**, 706, e9–720.

21. Tang, J., Yan, T., Bao, Y., Shen, C., Yu, C., Zhu, X., Tian, X., Guo, F., Liang, Q., Liu, Q. *et al.* (2019) LncRNA GLCC1 promotes colorectal carcinogenesis and glucose metabolism by stabilizing c-myc. *Nat. Commun.*, **10**, 3499-019-11447-8.

22. Swier, L.J.Y.M., Dzikiewicz-Krawczyk, A., Winkle, M., van den Berg, A. and Kluiver, J. Intricate crosstalk between MYC and noncoding RNAs regulates hallmarks of cancer. *Mol. Oncol.*, **13**, 26–45. https://doi.org/10.1002/1878-0261.12409.

23. Arman, K. and Möröy, T. (2020) Crosstalk between MYC and lncRNAs in hematological malignancies. *Front. Oncol.*, **10**, 579940.

24. Li, C., Kim, S.W., Rai, D., Bolla, A.R., Adhvaryu, S., Kinney, M.C., Robetorye, R.S. and Aguiar, R.C. (2009) Copy number abnormalities, MYC activity, and the genetic fingerprint of normal B cells mechanically define the microRNA profile of diffuse large B-cell lymphoma. *Blood*, **113**, 6681–6690.

25. Seitz, V., Butzhammer, P., Hirsch, B., Hecht, J., Gutgemann, I., Ehlers, A., Lenze, D., Oker, E., Sommerfeld, A., von der Wall, E. *et al.* (2011) Deep sequencing of MYC DNA-binding sites in burkitt lymphoma. *PLoS One*, **6**, e26837.

26. Ben-Porath, I., Thomson, M.W., Carey, V.J., Ge, R., Bell, G.W., Regev, A. and Weinberg, R.A. (2008) An embryonic stem cell-like gene expression signature in poorly differentiated aggressive human tumors. *Nat. Genet.*, **40**, 499–507.

27. Schuhmacher, M., Kohlhuber, F., Holzel, M., Kaiser, C., Burtscher, H., Jarsch, M., Bornkamm, G.W., Laux, G., Polack, A., Weidle, U.H. *et al.* (2001) The transcriptional program of a human B cell line in response to myc. *Nucleic Acids Res.*, **29**, 397–406.

28. Kazimierska, M., Podralska, M., Zurawek, M., Wozniak, T., Kasprzyk, M.E.Z., Sura, W., Losiewski, W., Ziolkowska-Suchanek, I., Kluiver, J., Van den Berg, A. *et al.* (2021) CRISPR/Cas9 screen for functional MYC binding sites reveals MYC-dependent vulnerabilities in K562 cells. *bioRxiv*.

29. Brinkman, E.K., Chen, T., Amendola, M. and van Steensel, B. (2014) Easy quantitative assessment of genome editing by sequence trace decomposition. *Nucleic Acids Res.*, **42**, e168.

30. Clark, M.B. and Mattick, J.S. (2011) Long noncoding RNAs in cell biology. *Semin. Cell Dev. Biol.*, **22**, 366–376.

31. Cabili, M.N., Dunagin, M.C., McClanahan, P.D., Biaesch, A., Padovan-Merhar, O., Regev, A., Rinn, J.L. and Raj, A. (2015) Localization and abundance analysis of human lncRNAs at single-cell and single-molecule resolution. *Genome Biol.*, **16**, 20-015-0586-4.

32. Yu, D., Cozma, D., Park, A. and Thomas-Tikhonenko, A. (2005) Functional validation of genes implicated in lymphomagenesis: an in vivo selection assay using a myc-induced B-cell tumor. *Ann. N. Y. Acad. Sci.*, **1059**, 145–159.

33. Fält, S., Merup, M., Tobin, G., Thunberg, U., Gahrton, G., Rosenquist, R. and Wennborg, A. (2005) Distinctive gene expression pattern in VH3-21 utilizing B-cell chronic lymphocytic leukemia. *Blood*, **106**, 681–689.

34. Hüttmann, A., Klein-Hitpass, L., Thomale, J., Deenen, R., Carpinteiro, A., Nückel, H., Ebeling, P., Führer, A., Edelmann, J., Sellmann, L. *et al.* (2006) Gene expression signatures separate B-cell chronic lymphocytic leukaemia prognostic subgroups defined by ZAP-70 and CD38 expression status. *Leukemia*, **20**, 1774–1782.

35. Schlosser, I., Holzel, M., Hoffmann, R., Burtscher, H., Kohlhuber, F., Schuhmacher, M., Chapman, R., Weidle, U.H. and Eick, D. (2005) Dissection of transcriptional programmes in response to serum and c-myc in a human B-cell line. *Oncogene*, **24**, 520–524.

36. Nie, Z., Hu, G., Wei, G., Cui, K., Yamane, A., Resch, W., Wang, R., Green, D.R., Tessarollo, L., Casellas, R. *et al.* (2012) C-myc is a universal amplifier of expressed genes in lymphocytes and embryonic stem cells. *Cell*, **151**, 68–79.

37. Lin, C.Y., Loven, J., Rahl, P.B., Paranal, R.M., Burge, C.B., Bradner, J.E., Lee, T.I. and Young, R.A. (2012) Transcriptional amplification in tumor cells with elevated c-myc. *Cell*, **151**, 56–67.

38. Wu, Z., Liu, X., Liu, L., Deng, H., Zhang, J., Xu, Q., Cen, B. and Ji, A. (2014) Regulation of lncRNA expression. *Cell. Mol. Biol. Lett.*, **19**, 561–575.

39. Kim, T., Jeon, Y.J., Cui, R., Lee, J.H., Peng, Y., Kim, S.H., Tili, E., Alder, H. and Croce, C.M. (2015) (2015) role of MYC-regulated long noncoding RNAs in cell cycle regulation and tumorigenesis. *J. Natl. Cancer Inst.*, **107**. https://doi.org/10.1093/jnci/dju505. Print.

40. Liu, C., Li, X., Hao, Y., Wang, F., Cheng, Z., Geng, H. and Geng, D. (2020) STAT1-induced upregulation of lncRNA KTN1-AS1 predicts poor prognosis and facilitates non-small cell lung cancer progression via miR-23b/DEPDC1 axis. *Aging (Albany NY)*, **12**, 8680–8701.

41. Zhang, Z.B. and Liu, N. (2021) Long non-coding RNA KTN1-AS1 promotes progression in pancreatic cancer through regulating microRNA-23b-3p/high-mobility group box 2 axis. *Aging (Albany NY)*, **13**, 20820–20835.

42. Li, C., Zhao, W., Pan, X., Li, X., Yan, F., Liu, S., Feng, J. and Lu, J. (2020) LncRNA KTN1-AS1 promotes the progression of non-small cell lung cancer via sponging of miR-130a-5p and activation of PDPK1. *Oncogene*, **39**, 6157–6171.

43. Jiang, Y., Wu, K., Cao, W., Xu, Q., Wang, X., Qin, X., Wang, X., Li, Y., Zhang, J. and Chen, W. (2020) Long noncoding RNA KTN1-AS1 promotes head and neck squamous cell carcinoma cell epithelial-mesenchymal transition by targeting miR-153-3p. *Epigenomics*, **12**, 487–505.

44. Mu, Y., Tang, Q., Feng, H., Zhu, L. and Wang, Y. (2020) lncRNA KTN1-AS1 promotes glioma cell proliferation and invasion by negatively regulating miR-505-3p. *Oncol. Rep.*, **44**, 2645–2655.

45. Dzikiewicz-Krawczyk, A., Kok, K., Slezak-Prochazka, I., Robertus, J.L., Bruining, J., Tayari, M.M., Rutgers, B., de Jong, D., Koerts, J., Seitz, A. *et al.* (2017) ZDHHC11 and ZDHHC11B are critical novel components of the oncogenic MYC-miR-150-MYB network in burkitt lymphoma. *Leukemia*, **31**, 1470–1473.

46. Hu, X., Xiang, L., He, D., Zhu, R., Fang, J., Wang, Z. and Cao, K. (2021) The long noncoding RNA KTN1-AS1 promotes bladder cancer tumorigenesis via KTN1 cis-activation and the consequent initiation of rho GTPase-mediated signaling. *Clin. Sci. (Lond)*, **135**, 555–574.

47. Xiang, J.F., Yin, Q.F., Chen, T., Zhang, Y., Zhang, X.O., Wu, Z., Zhang, S., Wang, H.B., Ge, J., Lu, X. *et al.* (2014) Human colorectal cancer-specific CCAT1-L lncRNA regulates long-range chromatin interactions at the MYC locus. *Cell Res.*, **24**, 513–531.

48. Hung, C.L., Wang, L.Y., Yu, Y.L., Chen, H.W., Srivastava, S., Petrovics, G. and Kung, H.J. (2014) A long noncoding RNA connects c-myc to tumor metabolism. *Proc. Natl. Acad. Sci. U. S. A.*, **111**, 18697–18702.

49. Zhang, P., Cao, L., Fan, P., Mei, Y. and Wu, M. (2016) LncRNA-MIF, a c-myc-activated long non-coding RNA, suppresses glycolysis by promoting Fbxw7-mediated c-myc degradation. *EMBO Rep.*, **17**, 1204–1220.

50. Yang, F., Xue, X., Zheng, L., Bi, J., Zhou, Y., Zhi, K., Gu, Y. and Fang, G. (2014) Long non-coding RNA GHET1 promotes gastric carcinoma cell proliferation by increasing c-myc mRNA stability. *FEBS J.*, **281**, 802–813.

51. Liao, L.M., Sun, X.Y., Liu, A.W., Wu, J.B., Cheng, X.L., Lin, J.X., Zheng, M. and Huang, L. (2014) Low expression of long noncoding XLOC_010588 indicates a poor prognosis and promotes proliferation through upregulation of c-myc in cervical cancer. *Gynecol. Oncol.*, **133**, 616–623.

52. Prensner, J.R., Chen, W., Han, S., Iyer, M.K., Cao, Q., Kothari, V., Evans, J.R., Knudsen, K.E., Paulsen, M.T., Ljungman, M. *et al.* (2014) The long non-coding RNA PCAT-1 promotes prostate cancer cell proliferation through cMyc. *Neoplasia*, **16**, 900–908.

53. Huang, J., Zhang, A., Ho, T.T., Zhang, Z., Zhou, N., Ding, X., Zhang, X., Xu, M. and Mo, Y.Y. (2016) Linc-RoR promotes c-myc expression through hnRNP I and AUF1. *Nucleic Acids Res.*, **44**, 3059–3069.

54. Hu, Y., Wang, F., Xu, F., Fang, K., Fang, Z., Shuai, X., Cai, K., Chen, J., Hu, P., Chen, D. *et al.* (2020) A reciprocal feedback of myc and lncRNA MTSS1-AS contributes to extracellular acidity-promoted metastasis of pancreatic cancer. *Theranostics*, **10**, 10120–10140.

55. Wang, L.W., Wang, Z., Ersing, I., Nobre, L., Guo, R., Jiang, S., Trudeau, S., Zhao, B., Weekes, M.P. and Gewurz, B.E. (2019) Epstein-barr virus subverts mevalonate and fatty acid pathways to promote infected B-cell proliferation and survival. *PLoS Pathog.*, **15**, e1008030.

56. Chen, L., Monti, S., Juszczynski, P., Ouyang, J., Chapuy, B., Neuberg, D., Doench, J.G., Bogusz, A.M., Habermann, T.M., Dogan, A. *et al.* (2013) SYK inhibition modulates distinct PI3K/AKT- dependent survival pathways and cholesterol biosynthesis in diffuse large B cell lymphomas. *Cancer Cell*, **23**, 826–838.

57. Nozaki, Y., Mitsumori, T., Yamamoto, T., Kawashima, I., Shobu, Y., Hamanaka, S., Nakajima, K., Komatsu, N. and Kirito, K. (2013) Rituximab activates syk and AKT in CD20-positive B cell lymphoma cells dependent on cell membrane cholesterol levels. *Exp. Hematol.*, **41**, 687–696.e1.

58. Sun, L., Shi, Y., Wang, G., Wang, X., Zeng, S., Dunn, S.E., Fairn, G.D., Li, Y.J. and Spaner, D.E. (2018) PPAR-delta modulates membrane cholesterol and cytokine signaling in malignant B cells. *Leukemia*, **32**, 184–193.

59. Gotoh, K., Kariya, R., Alam, M.M., Matsuda, K., Hattori, S., Maeda, Y., Motoyama, K., Kojima, A., Arima, H. and Okada, S. (2014) The antitumor effects of methyl-beta-cyclodextrin against primary effusion lymphoma via the depletion of cholesterol from lipid rafts. *Biochem. Biophys. Res. Commun.*, **455**, 285–289.

60. Reis-Sobreiro, M., Roue, G., Moros, A., Gajate, C., de la Iglesia-Vicente, J., Colomer, D. and Mollinedo, F. (2013) Lipid raft-mediated akt signaling as a therapeutic target in mantle cell lymphoma. *Blood Cancer. J.*, **3**, e118.

61. Uphoff, C.C. and Drexler, H.G. (2002) Detection of mycoplasma in leukemia-lymphoma cell lines using polymerase chain reaction. *Leukemia*, **16**, 289–293.

62. Swerdlow, S. (2008) WHO classification of tumours of haematopoietic and lymphoid tissues. *IARC.*.

63. Ennishi, D., Healy, S., Bashashati, A., Saberi, S., Hother, C., Mottok, A., Chan, F.C., Chong, L., Abraham, L., Kridel, R. *et al.* (2020) TMEM30A loss-of-function mutations drive lymphomagenesis and confer therapeutically exploitable vulnerability in B-cell lymphoma. *Nat. Med.*, **26**, 577–588.

64. Scott, D.W., Wright, G.W., Williams, P.M., Lih, C.J., Walsh, W., Jaffe, E.S., Rosenwald, A., Campo, E., Chan, W.C., Connors, J.M. *et al.* (2014) Determining cell-of-origin subtypes of diffuse large B-cell lymphoma using gene expression in formalin-fixed paraffin-embedded tissue. *Blood*, **123**, 1214–1217.

65. Tan, L.P., Wang, M., Robertus, J.L., Schakel, R.N., Gibcus, J.H., Diepstra, A., Harms, G., Peh, S.C., Reijmers, R.M., Pals, S.T. *et al.* (2009) miRNA profiling of B-cell subsets: specific miRNA profile for germinal center B cells with variation between centroblasts and centrocytes. *Lab. Investig.*, **89**, 708–716.

66. Danko, C.G., Hah, N., Luo, X., Martins, A.L., Core, L., Lis, J.T., Siepel, A. and Kraus, W.L. (2013) Signaling pathways differentially affect RNA polymerase II initiation, pausing, and elongation rate in cells. *Mol. Cell*, **50**, 212–222.

67. Sturn, A., Quackenbush, J. and Trajanoski, Z. (2002) Genesis: cluster analysis of microarray data. *Bioinformatics*, **18**, 207–208.

68. Mootha, V.K., Lindgren, C.M., Eriksson, K.F., Subramanian, A., Sihag, S., Lehar, J., Puigserver, P., Carlsson, E., Ridderstråle, M., Laurila, E. *et al.* (2003) PGC-1alpha-responsive genes involved in oxidative phosphorylation are coordinately downregulated in human diabetes. *Nat. Genet.*, **34**, 267–273.

69. Subramanian, A., Tamayo, P., Mootha, V.K., Mukherjee, S., Ebert, B.L., Gillette, M.A., Paulovich, A., Pomeroy, S.L., Golub, T.R., Lander, E.S. *et al.* (2005) Gene set enrichment analysis: a knowledge-based approach for interpreting genome-wide expression profiles. *Proc. Natl. Acad. Sci. U. S. A.*, **102**, 15545–15550.

70. Chen, E.Y., Tan, C.M., Kou, Y., Duan, Q., Wang, Z., Meirelles, G.V., Clark, N.R. and Ma'ayan, A. (2013) Enrichr: interactive and collaborative HTML5 gene list enrichment analysis tool. *BMC Bioinformatics*, **14**, 128.

71. Kuleshov, M.V., Jones, M.R., Rouillard, A.D., Fernandez, N.F., Duan, Q., Wang, Z., Koplev, S., Jenkins, S.L., Jagodnik, K.M., Lachmann, A. *et al.* (2016) Enrichr: a comprehensive gene set enrichment analysis web server 2016 update. *Nucleic Acids Res.*, **44**, W90–W97.

72. Goecks, J., Nekrutenko, A., Taylor, J. and Galaxy Team (2010) Galaxy: a comprehensive approach for supporting accessible, reproducible, and transparent computational research in the life sciences. *Genome Biol.*, **11**, R86 Epub 2010 Aug 25.

73. Blankenberg, D., Von Kuster, G., Coraor, N., Ananda, G., Lazarus, R., Mangan, M., Nekrutenko, A. and Taylor, J. (2010) Galaxy: a web-based genome analysis tool for experimentalists. *Curr. Protoc. Mol. Biol.*, **Chapter, 19**, Unit 19.10.1-21.

74. Haeussler, M., Schönig, K., Eckert, H., Eschstruth, A., Mianné, J., Renaud, J.B., Schneider-Maunoury, S., Shkumatava, A., Teboul, L., Kent, J. *et al.* (2016) Evaluation of off-target and on-target scoring algorithms and integration into the guide RNA selection tool CRISPOR. *Genome Biol.*, **17**, 148-016-1012-2.

75. Doench, J.G., Fusi, N., Sullender, M., Hegde, M., Vaimberg, E.W., Donovan, K.F., Smith, I., Tothova, Z., Wilen, C., Orchard, R. *et al.* (2016) Optimized sgRNA design to maximize activity and minimize off-target effects of CRISPR-Cas9. *Nat. Biotechnol.*, **34**, 184–191.

76. Sanjana, N.E., Shalem, O. and Zhang, F. (2014) Improved vectors and genome-wide libraries for CRISPR screening. *Nat. Methods*, **11**, 783–784.

77. Slezak-Prochazka, I., Kluiver, J., de Jong, D., Smigielska-Czepiel, K., Kortman, G., Winkle, M., Rutgers, B., Koerts, J., Visser, L., Diepstra, A. *et al.* (2016) Inhibition of the miR-155 target NIAM phenocopies the growth promoting effect of miR-155 in B-cell lymphoma. *Oncotarget*, **7**, 2391–2400.